Neuron
Article

An eIF4E1/4E-T Complex Determines the Genesis of Neurons from Precursors by Translationally Repressing a Proneurogenic Transcription Program

Guang Yang,[1] Craig A. Smibert,[2,3] David R. Kaplan,[1,3,*] and Freda D. Miller[1,3,4,*]
[1]Program in Neuroscience and Mental Health, Hospital for Sick Children, Toronto, ON M5G 1L7, Canada
[2]Department of Biochemistry
[3]Department of Molecular Genetics
[4]Department of Physiology
University of Toronto, Toronto, ON M5S 1A8, Canada
*Correspondence: dkaplan@sickkids.ca (D.R.K.), fredam@sickkids.ca (F.D.M.)
http://dx.doi.org/10.1016/j.neuron.2014.10.022

SUMMARY

Here, we have addressed the mechanisms that determine genesis of the correct numbers of neurons during development, focusing on the embryonic cortex. We identify in neural precursors a repressive complex involving eIF4E1 and its binding partner 4E-T that coordinately represses translation of proteins that determine neurogenesis. This eIF4E1/4E-T complex is present in granules with the processing body proteins Lsm1 and Rck, and disruption of this complex causes premature and enhanced neurogenesis and neural precursor depletion. Analysis of the 4E-T complex shows that it is highly enriched in mRNAs encoding transcription factors and differentiation-related proteins. These include the proneurogenic bHLH mRNAs, which colocalize with 4E-T in granules and whose protein products are aberrantly upregulated following knockdown of eIF4E, 4E-T, or processing body proteins. Thus, neural precursors are transcriptionally primed to generate neurons, but an eIF4E/4E-T complex sequesters and represses translation of proneurogenic proteins to determine appropriate neurogenesis.

INTRODUCTION

Developmental genesis of the correct numbers and types of mammalian neurons involves a tightly regulated interplay between mechanisms intrinsic to neural precursors and the environment that surrounds them. These interactions ensure that neurons are generated appropriately and that neural precursors are not prematurely exhausted, since the same precursor pool also generates astrocytes, oligodendrocytes, and adult neural stem cells. When this process is disrupted, as in some neurodevelopmental disorders, it causes aberrant neural circuit formation and cognitive dysfunction (Gauthier et al., 2007; Wang et al., 2010).

Transcriptional regulation is one mechanism that plays a key role in determining neurogenesis. For example, sustained expression of proneurogenic basic-helix-loop-helix (bHLH) transcription factors like the neurogenins is necessary for mammalian cortical precursors to make neurons (Bertrand et al., 2002; Imayoshi and Kageyama, 2014). Intriguingly, recent data suggest that translational regulation is also important. For example, the RNA-binding protein Staufen2 asymmetrically localizes mRNAs in cortical radial glial precursors, thereby promoting maintenance of the stem cell state (Vessey et al., 2012; Kusek et al., 2012). As a second example, the translational regulator eIF4E1 has been implicated in autism spectrum disorder (ASD) in humans (Neves-Pereira et al., 2009), and increasing neural eIF4E function caused aberrant circuitry and ASD-like behavior in mice (Santini et al., 2013; Gkogkas et al., 2013).

How might eIF4E-dependent translational regulation determine neurogenesis? Mammalian cells express three eIF4E family members (eIF4E1–eIF4E3) that can both initiate and suppress translation in response to extracellular signals (Rhoads, 2009). eIF4E1, the best studied eIF4E, initiates translation by binding the 5′ cap of mRNA and the scaffolding protein eIF4G (Jackson et al., 2010). eIF4E1 can be sequestered from eIF4G and positive initiation complexes by eIF4E binding proteins 1–3 (Sonenberg and Hinnebusch, 2009). eIF4E is also present in multiprotein complexes that repress translation such as the fragile X mental retardation protein (FMRP)/CYFIP1 complex that suppresses FMRP target mRNAs at synapses (Napoli et al., 2008). eIF4E1 also binds a protein called 4E-T that associates with granules that silence translation called processing bodies, or P-bodies (Ferraiuolo et al., 2005; Eulalio et al., 2007). Thus, eIF4E proteins, depending on the complexes they form, can either initiate translation or specifically suppress the translation of subsets of mRNAs.

Here, we have asked whether translational regulation is important for genesis of neurons in the embryonic cortex. We identify an eIF4E1/4E-T complex that is present in P-body-like granules in neural precursors and that coordinately represses translation of proneurogenic proteins to maintain the stem cell state while, at the same time, allowing neurogenesis. These findings suggest that neural precursors are transcriptionally primed to generate

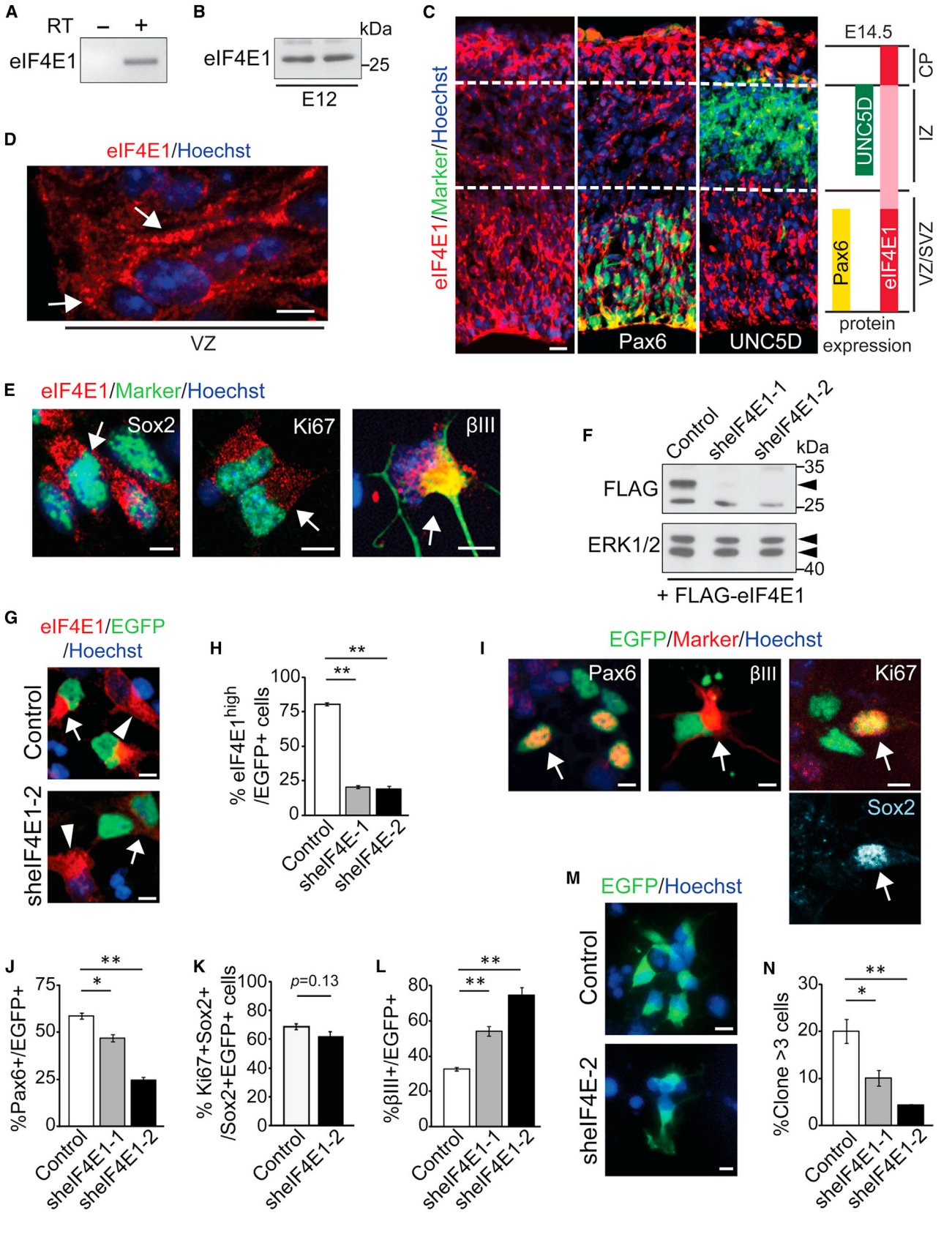

(legend on next page)

neurons, and an eIF4E1/4E-T complex sequesters and represses translation of mRNAs encoding proneurogenic proteins to ultimately determine appropriate neurogenesis.

RESULTS

Decreasing eIF4E1 Induces Neurogenesis at the Expense of Cortical Radial Precursor Maintenance

To ask about eIF4E during cortical development, we analyzed its expression. RT-PCR and western blots showed that eIF4E1 was expressed in the E11/12 cortex (Figures 1A and 1B). Immunostaining of E14.5 cortical sections showed robust eIF4E1 expression in ventricular and subventricular zones (VZ/SVZ) (Figure 1C), where it localized to punctate cytoplasmic granules in radial precursors expressing Pax6 (Figures 1C and 1D). eIF4E1 was also detectable in neurons of the cortical plate (CP) but was lower in the intermediate zone (IZ), which contains UNC5D-positive migrating newborn neurons (Figure 1C). Immunostaining of E12.5 precursors cultured for 3 days confirmed that eIF4E1 was localized to punctate foci in Sox2- and Ki67-positive proliferating precursors and in βIII-tubulin-positive neurons (Figure 1E).

We asked about eIF4E1 function with two small hairpin RNAs (shRNAs) that knocked down expression of a FLAG-tagged murine eIF4E1 when cotransfected into human embryonic kidney 293 (HEK293) cells (Figure 1F). We cotransfected cultured precursors with these shRNAs and a nuclear EGFP expression plasmid. Three days later, eIF4E1 immunoreactivity was significantly reduced in cells transfected with eIF4E1 but not control shRNA (Figures 1G and 1H). eIF4E1 knockdown had no effect on cell survival, as indicated by EGFP-positive cells with condensed apoptotic nuclei (control shRNA, 10.1% ± 0.6%; eIF4E shRNA1, 11.4% ± 0.5%; eIF4E shRNA2, 14.2% ± 1.1%). It did, however, decrease EGFP-positive, Pax6-positive radial precursors (Figures 1I and 1J), although the precursor proliferation index was unaffected, as monitored by double labeling for Sox2 and Ki67 (Figures 1I and 1K). In contrast, EGFP-positive βIII-tubulin neurons were increased by eIF4E1 knockdown (Figures 1I and 1L). Since almost all EGFP-positive cells expressed either Pax6 or βIII-tubulin (92%–100% in all conditions; Figures 1J and 1L), then this indicates that eIF4E1 knockdown depletes radial precursors by promoting their differentiation to neurons.

Further support for this conclusion came from clonal analysis performed using the *piggybac* (PB) transposon to stably express EGFP in cultured precursors (Tsui et al., 2013; Zander et al., 2014). E12.5 cortical precursors were cotransfected at low efficiency (at most, 1% to 3%) with control or eIF4E1 shRNAs plus plasmids encoding PB transposase and the PB EGFP reporter. Immunostaining 3 days later showed that clone size, indicative of self-renewal, was significantly smaller following eIF4E1 knockdown (Figures 1M and 1N).

An eIF4E1 Complex Maintains Radial Precursors In Vivo by Binding mRNAs

To ask if eIF4E1 regulates neurogenesis in vivo, we electroporated E13/14 cortices in utero with a nuclear EGFP expression plasmid and eIF4E1 shRNA2, thereby transfecting radial precursors that generate neurons in the VZ/SVZ that subsequently migrate through the IZ to the CP (Gauthier et al., 2007). Immunostaining 3 days later showed that eIF4E1 knockdown perturbed the location of EGFP-positive cells, with fewer in the VZ/SVZ and CP and more in the IZ (Figures 2A and 2B). eIF4E1 knockdown also robustly decreased EGFP-positive, Pax6-positive radial precursors and Ki67-positive proliferating precursors, although, as seen in culture, the radial precursor proliferation index (Ki67-positive, Pax6-positive, EGFP-positive/Pax6-positive, EGFP-positive cells) was unaffected (Figures 2C–2G; Figures S1A and S1B available online).

To ask if neurons were coincidentally increased, we analyzed the cortical neuron markers Satb2, Ctip2, and Tbr1 (Figure 2H; Figures S1C–S1H). As we previously reported (Tsui et al., 2013), almost all EGFP-positive neurons generated over this time frame expressed Satb2, and very few expressed Ctip2 or Tbr1 (Figures 2H and 2I). eIF4E1 knockdown did not affect Ctip2- or Tbr1-positive neurons, but it significantly increased those expressing Satb2 (Figures 2H and 2I) or βIII-tubulin (Figure 2K). The magnitude of the neuronal increase was similar to that of the radial precursor decrease (22% versus 19% of total EGFP-positive cells, respectively). In addition, almost all

Figure 1. eIF4E1 Is Expressed in the Embryonic Cortex and Regulates Cortical Precursor Self-Renewal versus Differentiation in Culture

(A) RT-PCR (RT) for eIF4E1 mRNA in the E11/12 cortex. Minus symbol indicates no reverse transcriptase.

(B) Western blot of eIF4E1 in the E11/12 cortex. Molecular weight marker sizes (in kilodaltons; kDa) are shown at the right.

(C and D) E14.5 coronal cortical sections immunostained for eIF4E1 (red). In (C), sections were costained for Pax6 or UNC5D (both green), and cortical boundaries are shown with white lines. (D) A high-magnification confocal image of the VZ, with arrows highlighting eIF4E1-positive granules.

(E) Cortical cultures were immunostained for eIF4E1 (red) and Sox2, Ki67, or βIII-tubulin (all green). Arrows denote marker-positive cells.

(F) Western blots of HEK293 cells cotransfected with a FLAG-tagged mouse eIF4E1 construct and control shRNA, or one of two eIF4E1 shRNAs (sheIF4E1-1, sheIF4E1-2). The blot was probed for FLAG and reprobed for Erk1/2 as a loading control. Arrowheads indicate target proteins.

(G–L) Cultured E12.5 cortical precursors were cotransfected with EGFP and control or eIF4E1 shRNAs (sheIF4E1-1 or sheIF4E1-2) for 3 days. (G and H) Precursors were immunostained for eIF4E1 (red) and EGFP (green) (G) and quantified for relative levels of immunodetectable eIF4E1 (H). Arrows and arrowheads denote EGFP-positive and -negative cells, respectively. $^{**}p < 0.01$; n = 3 experiments. (I) Precursors immunostained for EGFP (green) and Pax6, βIII-tubulin, or Ki67 (all red). Cells on top right were triple labeled for Sox2 (bluish white, bottom right). Arrows denote double- or triple-labeled cells. (J–L) Quantification of cultures as in (I) for EGFP-positive, Pax6-positive cells (J), for the proportion of Sox2-positive, EGFP-positive cells that expressed Ki67 (K), or for EGFP-positive, βIII-tubulin-positive cells (L). $^{*}p < 0.05$; $^{**}p < 0.01$; n = 3 experiments.

(M and N) E12.5 cortical precursors were cotransfected with the piggyBac plasmids and control or eIF4E1 shRNA. Precursors were immunostained 3 days later for EGFP (green, M), and clones containing three or more EGFP-positive cells quantified (N). $^{*}p < 0.05$; $^{**}p < 0.01$; n = 3 experiments.

Sections or cells in (C), (D), (E), (G), (I), and (M) were counterstained with Hoechst (blue). Scale bars, 30 μm in (C) and 5 μm in (D), (E), (I), and (M). Error bars denote SEM.

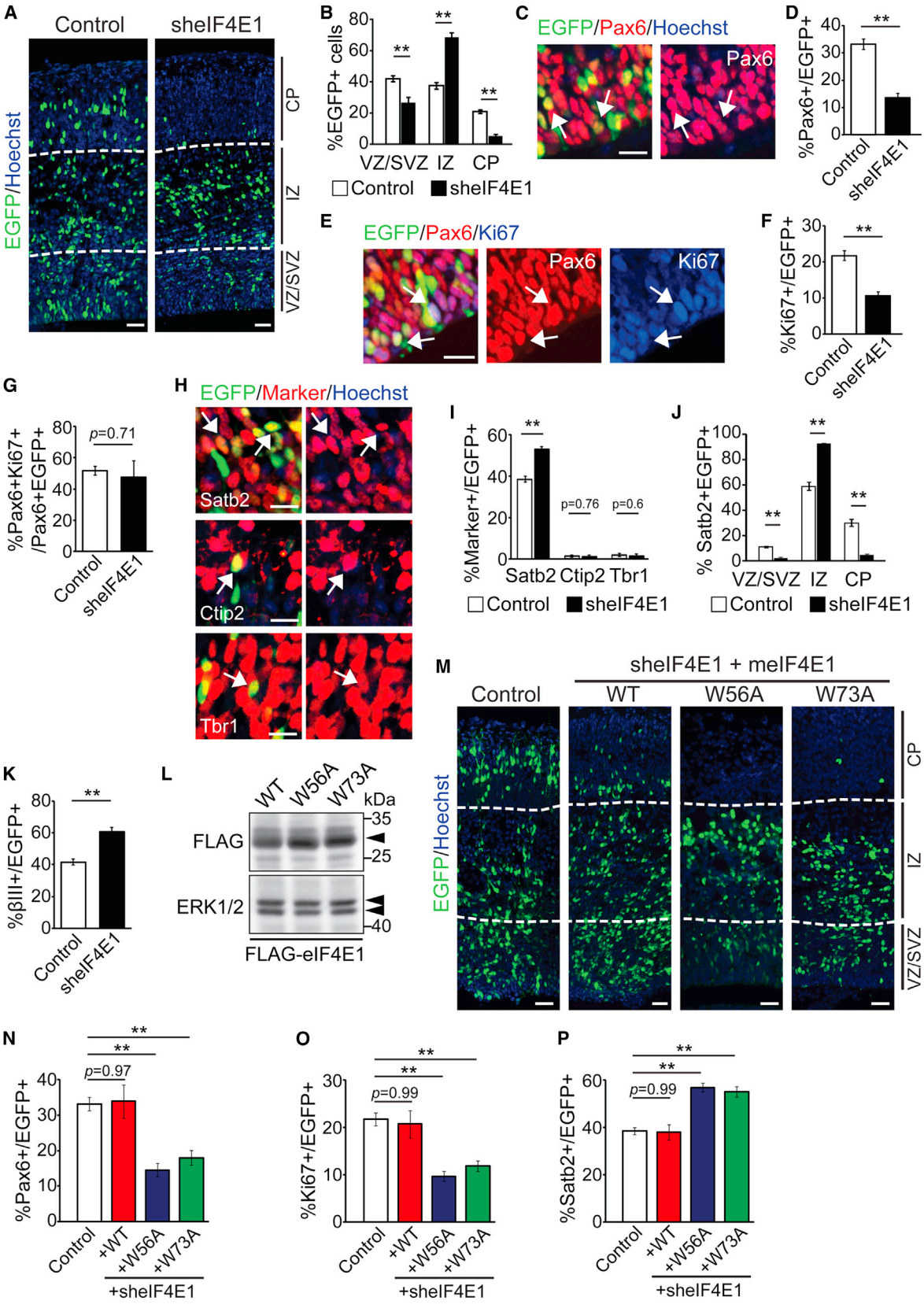

(legend on next page)

EGFP-positive neurons were mislocalized to the IZ following eIF4E1 knockdown (Figure 2J; Figure S1C).

To ensure the specificity of these phenotypes, we performed rescue experiments with an shRNA-resistant wild-type murine eIF4E1. We also performed rescue experiments with eIF4E1 proteins that were mutated to prevent binding to mRNA (W56A mutant) or to protein partners that mediate translational activation or suppression (W73A mutant) (Ferraiuolo et al., 2005). We confirmed that these proteins were expressed equally well (Figure 2L) and electroporated them with eIF4E1 shRNA into the E13/14 cortex. Analysis 3 days later showed that wild-type eIF4E1, but not the two mutant eIF4E1s (which were also shRNA resistant), rescued the aberrant location of EGFP-positive cells caused by eIF4E1 knockdown (Figure 2M; Figure S1I). Wild-type, but not mutant, eIF4E1s also rescued EGFP-positive, Pax6-positive, and Ki67-positive proliferating precursors and Satb2-positive neurons to control levels (Figures 2N–2P). These experiments validate the eIF4E1 knockdown phenotype and show that eIF4E1 must form a complex with a protein partner and bind to mRNAs to inhibit neurogenesis.

Decreasing eIF4G1, which Is Required for the Positive Translational Actions of eIF4E1, Has the Opposite Effect, Maintaining Precursors and Decreasing Neurogenesis

These data indicate a critical role for eIF4E1 but do not distinguish its roles in translational activation versus repression. To do this, we examined eIF4G, a necessary eIF4E partner for translation initiation (Sonenberg and Hinnebusch, 2009). Immunostaining showed that eIF4G was localized to punctate cytoplasmic foci in radial precursors of the E14.5 cortical VZ/SVZ (Figures 3A and 3B). To ask about its functional role, we used murine eIF4G1 shRNAs that were validated in HEK293 cells (Figure 3C). We electroporated E13/14 cortices with the most efficacious of these (eIF4G1 shRNA1) and analyzed sections 3 days later. eIF4G1 knockdown increased EGFP-positive, Pax6-positive radial precursors in the VZ/SVZ (Figures 3D–3F; Figure S2). However, the proliferation index of these radial precursors was reduced (Figure 3G). In addition, EGFP-positive, Satb2-positive neurons were decreased (Figure 3H). Thus, eIF4G1 knockdown decreased the proliferation and differentiation of radial precursors, a phenotype that is different from that seen following eIF4E1 knockdown.

These findings suggest that the enhanced neurogenesis seen following eIF4E1 knockdown might be due to derepression of translation of proneurogenic mRNAs. If so, then coincident eIF4G knockdown might inhibit this aberrant proneurogenic translation and rescue the eIF4E knockdown phenotype. To test this idea, we coelectroporated E13/14 cortices with shRNAs for both eIF4E1 and eIF4G1. Analysis 3 days later showed that coincident eIF4G1 knockdown normalized the aberrant distribution of EGFP-positive cells seen with eIF4E1 knockdown (Figures 3I and 3J) and rescued EGFP-positive, Pax6-positive precursors and Satb2-positive neurons to control levels (Figures 3K and 3L).

The Translational Repressor 4E-T Associates with eIF4E1, and This Complex Is Spatially Distinct from the eIF4E1/eIF4G Complex

The data obtained with the W73A eIF4E1 protein binding mutant (Figures 2M–2P) suggest that eIF4E1 binds to a protein partner to repress neurogenesis and maintain radial precursors. We asked whether this was 4E-T since it binds to the eIF4E1 W73 site (Ferraiuolo et al., 2005; Kamenska et al., 2014). Western blots showed expression of 4E-T in the E12 cortex (Figure 4A), and immunostaining showed that it was expressed in the same cells as eIF4E1 in the E15.5 VZ/SVZ (Figure 4B).

To ask whether 4E-T was bound to eIF4E1 in the embryonic cortex, we used two approaches. First, we performed coimmunoprecipitation experiments, after confirming that the 4E-T antibody immunoprecipitated 4E-T from the embryonic cortex (Figure S3A). Immunoprecipitation of E12.5 cortical lysates with anti-4E-T followed by western blotting showed that eIF4E1 was present in the 4E-T immunoprecipitates (Figure 4C). Second, we double-labeled E14.5 cortical sections with antibodies for 4E-T and eIF4E1. These proteins were colocalized in a subpopulation of punctate cytoplasmic foci in radial precursor cell bodies and apical endfeet adjacent to the ventricle (Figure 4D).

Since 4E-T and eIF4G both bind eIF4E1 at the W73 site, we asked about the relative distribution of granules containing these three proteins. Triple labeling of cultured precursors showed that many fewer foci were positive for 4E-T than for either eIF4E1 or

Figure 2. eIF4E1 Knockdown In Vivo Increases Neurogenesis and Depletes Radial Precursors

(A–K) E13/14 cortices were coelectroporated with EGFP and control or eIF4E1 shRNAs, and coronal cortical sections were analyzed 3 days later. (A and B) Sections were immunostained for EGFP (green, A), and the relative location of EGFP-positive cells was quantified (B). $^{**}p < 0.01$; n = 3 embryos each. (C) Images of the VZ/SVZ from control electroporated sections immunostained for EGFP (green) and Pax6 (red). Arrows denote double-labeled cells. (D) Quantification of sections as in (C) for EGFP-positive, Pax6-positive cells. $^{**}p < 0.01$; n = 3 embryos each. (E) Images of the VZ/SVZ from control electroporated sections immunostained for EGFP (green), Pax6 (red), and Ki67 (blue). Arrows denote triple-labeled cells. (F and G) Quantification of sections as in (E) for EGFP-positive, Ki67-positive cells (F) or for the proportion of EGFP-positive, Pax6-positive cells that also expressed Ki67 (G). $^{**}p < 0.01$; n = 3 embryos each. (H) Images of the CP from control electroporated sections immunostained for EGFP (green) and Satb2, Ctip2, or Tbr1 (all red). Arrows denote double-labeled cells. (I and J) Quantification of sections as in (H) for EGFP-positive cells that expressed Satb2, Ctip2, or Tbr1 (I) or for the relative location of EGFP-positive, Satb2-positive cells (J). $^{**}p < 0.01$; n = 3 embryos each. (K) Quantification of immunostained sections for EGFP-positive, βIII-tubulin-positive cells. $^{**}p < 0.01$; n = 3 embryos each.

(L) Western blots of HEK293 cells transfected with wild-type, W56A, or W73A FLAG-tagged mouse eIF4E1. The blot was probed for FLAG and reprobed for Erk1/2. Arrowheads indicate the target proteins.

(M–P) E13/14 cortices were coelectroporated with control or eIF4E1 shRNA, and wild-type (WT), W56A, or W73A eIF4E1, and coronal cortical sections were analyzed 3 days later. (M) Sections immunostained for EGFP (green). (N–P) Quantification of immunostained sections for EGFP-positive cells that expressed Pax6 (N), Ki67 (O), or Satb2 (P). $^{**}p < 0.01$; $n \geq 3$ embryos each.

Sections in (A), (C), (H), and (M) were counterstained with Hoechst (blue). Scale bars, 50 μm in (A) and (M) and 20 μm in (C), (E), and (H). Error bars denote SEM. See also Figure S1.

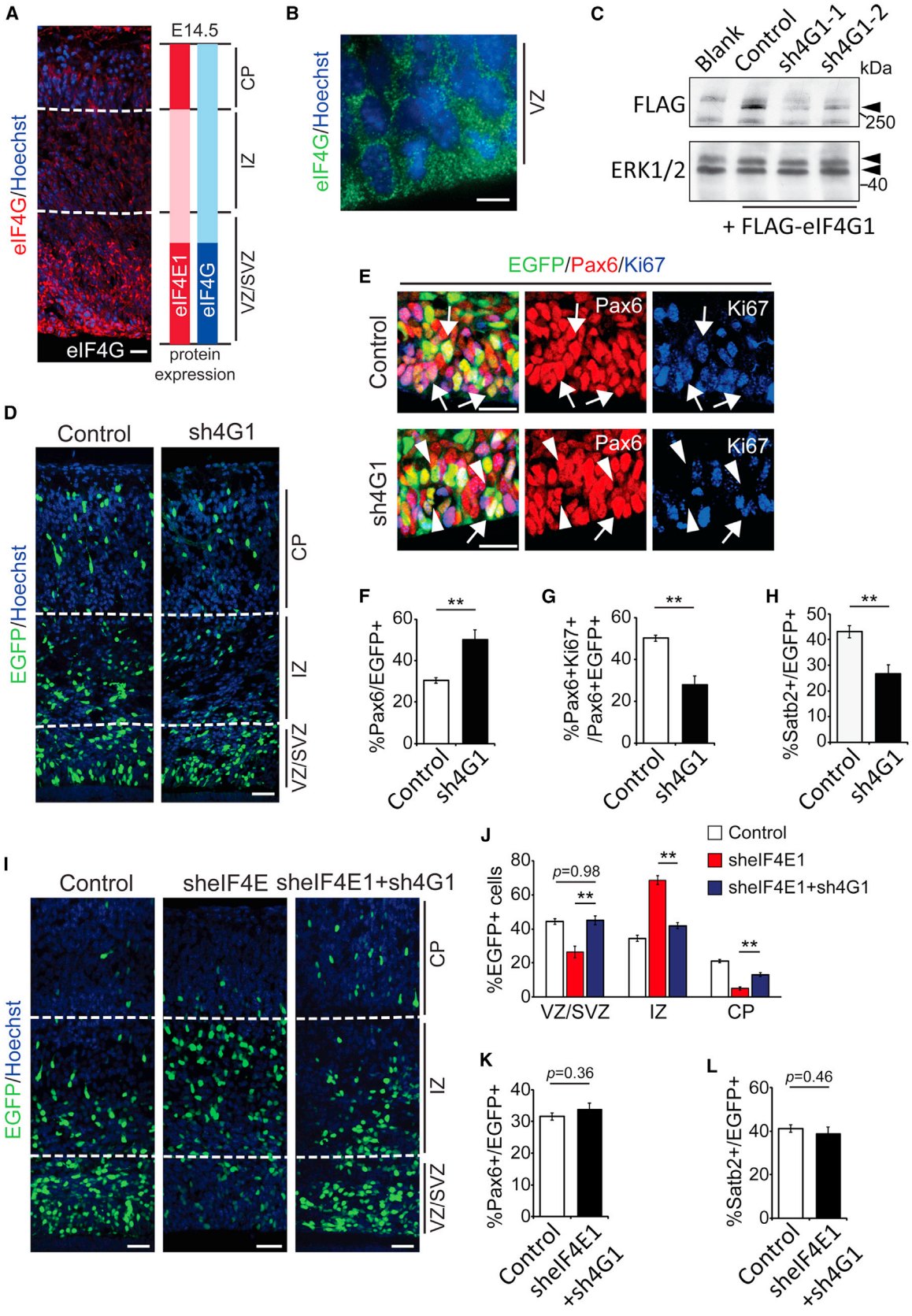

(legend on next page)

eIF4G (Figure 4E; Figure S3B). Almost 70% of 4E-T-positive foci were positive for eIF4E1, but almost none were positive for eIF4G (Figure 4F). Conversely, only 2.7% ± 0.4% of eIF4E1-positive foci were positive for 4E-T (Figure 4E; Figure S3B). An additional 10.3% ± 0.8% of the eIF4E1-positive foci were positive for eIF4G, but most eIF4E1 foci were negative for both eIF4G and 4E-T (Figure 4E; Figure S3B), as previously seen in cell lines (Rau et al., 1996; Ferraiuolo et al., 2005). Thus, 4E-T is present in a distinct population of granules, most of which contain eIF4E1 but not eIF4G.

4E-T Maintains Precursors and Inhibits Neurogenesis and Requires Binding to eIF4E to Do So

To test the idea that 4E-T might be the relevant repressive eIF4E1 binding partner, we used 4E-T shRNAs that knocked down cotransfected murine 4E-T in HEK293 cells (Figure 4G). When one of these shRNAs (4E-T shRNA2) was transfected into cultured precursors, it effectively reduced the bright 4E-T-positive granules present in control cells (Figure 4H; Figure S3C). We electroporated this 4E-T shRNA into E13/14 cortices and immunostained sections 3 days later. 4E-T knockdown decreased EGFP-positive cells in the VZ/SVZ and increased those in the CP (Figure 4I; Figure S3D), coincident with a decrease in EGFP-positive proliferating radial precursors (Figures 4J and 4K) and an increase in EGFP-positive, Satb2-positive, and βIII-tubulin-positive neurons (Figures 4L and 4M). As for eIF4E1 knockdown, Ctip2-positive and Tbr1-positive neurons were unaffected (Figure 4L; Figure S3E). Thus, 4E-T normally inhibits genesis of neurons from radial precursors.

To ask if 4E-T requires binding to eIF4E to inhibit neurogenesis, we performed rescue experiments with shRNA-resistant constructs encoding wild-type 4E-T and mutant 4E-T incapable of binding eIF4E (Y30A mutant) (Ferraiuolo et al., 2005). We showed that both 4E-T proteins were expressed equally well (Figure 4N) and then coelectroporated them with 4E-T shRNA into E13/14 cortices. Analysis 3 days later showed that wild-type, but not Y30A, 4E-T normalized all of the 4E-T knockdown-induced phenotypes, including the aberrant distribution of EGFP-positive cells (Figure 4O; Figure S3F), the decrease in proliferating radial precursors (Figures 4P and 4Q) and the increase in Satb2-positive neurons (Figure 4R). These data validate the specificity of the 4E-T knockdown phenotype and indicate that 4E-T requires binding to eIF4E to repress neurogenesis.

eIF4E1 and 4E-T Are Each Sufficient to Enhance Precursor Maintenance and Inhibit Neurogenesis

These data suggest that an eIF4E1/4E-T complex is necessary to maintain radial precursors. To further test this idea, we overexpressed eIF4E1 and 4E-T, electroporating them into E13/14 cortices. Analysis 3 days later showed that eIF4E1 and 4E-T both significantly increased EGFP-positive cells in the VZ/SVZ (Figures S4A–S4C). eIF4E1 or 4E-T overexpression also caused a significant increase in Pax6-positive radial precursors (Figure 5A) and a decrease in Satb2-positive neurons (Figure 5B). Thus, eIF4E1 and 4E-T are each sufficient to maintain precursors and repress neurogenesis.

The P-body Proteins Lsm1 and Rck Are Necessary to Localize 4E-T and to Repress Neurogenesis

4E-T is thought to repress translation, in part, by association with P-bodies (Andrei et al., 2005; Eulalio et al., 2007; Ferraiuolo et al., 2005). To ask if eIF4E1 and 4E-T were associated with P-bodies in radial precursors, we analyzed two P-body proteins, the RNA-binding complex protein Lsm1 and the Dead box RNA helicase Rck/p54 (Eulalio et al., 2007). Immunostaining showed that Lsm1 and Rck were present in cultured precursors, where they were highly colocalized with 4E-T (Figure 5C); almost all 4E-T-positive foci were colabeled for Lsm1 or Rck, while most Lsm1-positive or Rck-positive foci were colabeled for 4E-T (Figure 5D). Moreover, more than half of the Lsm1 granules also colabeled for eIF4E1, and almost none were colabeled for eIF4G (Figures 5E and 5F). Thus, radial precursors contain a P-body-like complex that includes 4E-T, Lsm1, and Rck, and more than half of the 4E-T-containing granules also contain eIF4E1 but not eIF4G.

In cell lines, Lsm1 is required for P-body formation and for 4E-T association with P-bodies (Andrei et al., 2005; Novotny et al., 2012). To ask if Lsm1 was necessary for 4E-T P-body association in radial precursors, we used an Lsm1 shRNA that knocked down FLAG-tagged murine Lsm1 when cotransfected in HEK293 cells (Figure 5G). Cultured precursors were transfected with Lsm1 shRNA and immunostained 3 days later (Figure 5H). Lsm1 knockdown reduced the number of 4E-T-positive granules per cell almost 3-fold (Figure 5I).

These data suggest that P-body-like granules might be necessary for the repressive eIF4E1/4E-T complex in radial precursors. To test this idea, we electroporated E13/14 cortices with shRNAs for Lsm1 or Rck (Figure 5G) and immunostained sections 3 days

Figure 3. eIF4G1 Knockdown Does the Opposite of eIF4E1 Knockdown, Enlarging the Precursor Pool and Decreasing Neurogenesis

(A and B) Coronal E14.5 cortical sections immunostained for eIF4G (red in A, green in B). (B) shows the VZ at higher magnification.

(C) Western blots of HEK293 cells (Blank) cotransfected with FLAG-tagged mouse eIF4G1 and control or eIF4G1 shRNAs (sh4G1-1 or sh4G1-2). The blot was probed for FLAG and reprobed for Erk1/2. Arrowheads denote target proteins.

(D–H) E13/14 mouse cortices were coelectroporated with nuclear EGFP and control or eIF4G1 shRNA1 (sh4G1), and coronal cortical sections were analyzed 3 days later. (D) Sections immunostained for EGFP (green). (E) Images of the VZ/SVZ immunostained for EGFP (green), Pax6 (red), and Ki67 (blue). Arrows denote triple-labeled cells and arrowheads denote EGFP-positive, Pax6-positive, Ki67-negative cells. (F and G) Quantification of sections as in (E) for EGFP-positive, Pax6-positive cells (F) and for EGFP-positive, Pax6-positive cells that expressed Ki67 (G). $^{**}p < 0.01$; n = 4 embryos each. (H) Quantification of immunostained sections for EGFP-positive, Satb2-positive cells. $^{**}p < 0.01$; n = 4 embryos each.

(I–L) E13/14 cortices were coelectroporated with EGFP and control or eIF4E1 shRNA plus or minus the eIF4G1 shRNA1. Coronal cortical sections were analyzed 3 days later. (I and J) Sections were immunostained for EGFP (green, I) and EGFP-positive cells in different cortical regions quantified (J). $^{**}p < 0.01$; $n \geq 3$ embryos each. (K and L) Quantification of immunostained sections for EGFP-positive cells that expressed Pax6 (K) or Satb2 (L). $n \geq 5$ embryos each.

Sections in (A), (B), (D), and (I) were counterstained with Hoechst (blue). Scale bars, 50 μm in (A), (D), and (I); 30 μm in (E), and 5 μm in (B). Error bars denote SEM. See also Figure S2.

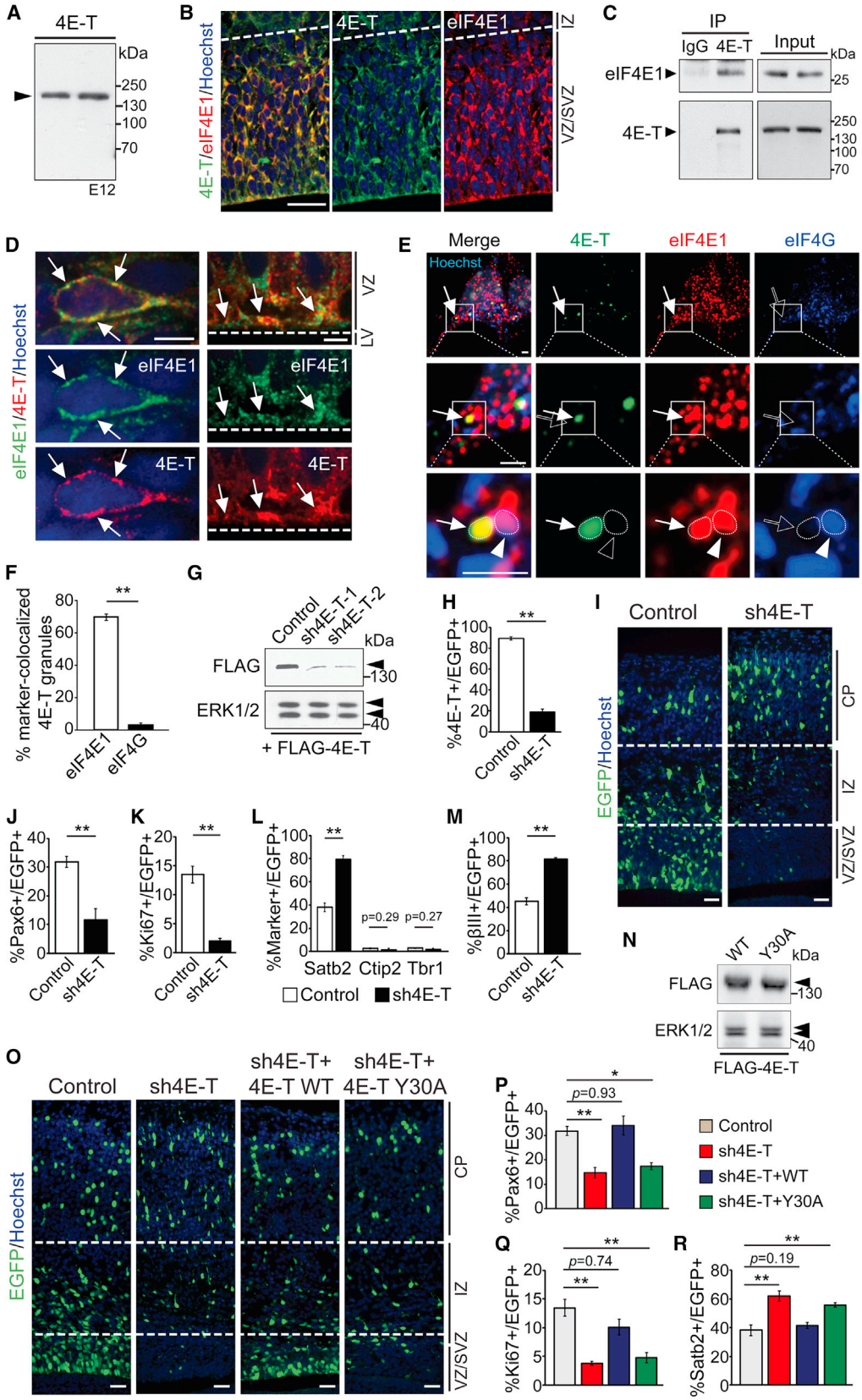

(legend on next page)

later. As seen with knockdown of eIF4E or 4E-T, Lsm1 and Rck knockdown depleted EGFP-positive cells from the VZ/SVZ (Figures 5J and 5K), decreased EGFP-positive Pax6- or Ki67-positive radial precursors (Figures 5L and 5M), and increased Satb2-positive neurons (Figure 5N).

4E-T Is Highly Enriched for Binding to mRNAs Encoding Transcription Factors Such as the Proneurogenic bHLHs

These findings suggest that an eIF4E/4E-T complex localizes and represses translation of mRNAs that promote neurogenesis. Therefore, we isolated 4E-T-binding mRNAs from the E12/13 cortex, focusing on 4E-T since only a small proportion (3%) of the total eIF4E1 foci in radial precursors contained 4E-T. To do this, we immunoprecipitated cortical lysates with anti-4E-T and analyzed coimmunoprecipitated mRNAs by microarrays (Gene Expression Omnibus [GEO] accession number GSE61729). To control for nonspecific binding, we performed similar immunoprecipitations with control immunoglobulin G (IgG). We focused on transcripts that were at least 1.5-fold enriched in the 4E-T immunoprecipitates relative to the total input lysate and that were absent from the control IgG immunoprecipitates (see Experimental Procedures). This approach identified 1,545 4E-T-enriched precipitated mRNAs, of which 1,439 encoded known proteins (Table S1). Analysis of this latter group (Figure 6A) showed that the top six gene ontology categories were transcriptional regulators, with a particularly robust enrichment for transcription factors; of 1,439 4E-T target mRNAs, 253 (or 17.6%) were transcription factors. The next nine categories all had to do with cell differentiation, proliferation, and migration, with a particularly robust enrichment in mRNAs associated with differentiation of neural stem cells and the differentiation, development, and migration of neurons (Figure 6A).

To analyze these mRNAs further, we categorized them into those involved in gene expression, cellular development, and cell growth and proliferation and looked at the overlap between these categories using a Venn diagram (Figure 6B). One hundred fifty-three of the mRNAs in these groups encoded proteins that were included in all three categories, and more than half of these encoded transcription factors (Figure 6C). Many of these transcription factors have been previously implicated in the regulation of neurogenesis, as shown by a heatmap (Figure 6D).

To validate these findings, we focused on a subset of 4E-T-associated mRNAs that encoded neurogenic bHLHs known to be essential for cortical neurogenesis: *ascl1*, *neurod1*, *neurod4*, *neurogenin1*, and *neurogenin2* mRNAs. We first used quantitative PCR (qPCR) to analyze their relative levels in three independent immunoprecipitates each with the 4E-T antibody and the nonspecific IgG. As controls, we performed a similar analysis for (1) *godz* and *eIF4E* mRNAs, which were not enriched in the 4E-T immunoprecipitates; (2) *sprouty2* mRNA, which was robustly enriched; and (3) *rpl27a* mRNA, which was significantly decreased (Table S1). This analysis validated the microarray data and showed that all of the neurogenic bHLH mRNAs were enriched in the 4E-T immunoprecipitates, with at least a 4-fold enrichment for all except *ascl1* (Figure 6E). In contrast, *godz* and *eIF4E* mRNAs were unchanged, and *rpl27a* mRNA was lower in the immunoprecipitates (Figure 6E). A comparison of the relative fold enrichment seen on the microarrays and by qPCR showed excellent correspondence between the two approaches (Figure 6F).

4E-T Colocalizes with Proneurogenic bHLH mRNAs, and These Complexes Are Enriched in Precursors that Do Not Express Proneurogenic Proteins

Since *neurod1*, *neurogenin2*, and *neurogenin1* mRNAs were all enriched more than 4-fold in 4E-T immunoprecipitates, we asked whether they colocalized with 4E-T in radial precursors in vivo. To do this, we performed fluorescent in situ hybridization

Figure 4. eIF4E1 Interacts with 4E-T in Radial Precursors, and This Complex Is Essential to Inhibit Neuronal Differentiation

(A) Western blot for 4E-T (arrowhead) in E12 cortex.

(B) Images of the E14.5 cortical VZ/SVZ immunostained for eIF4E1 (red) and 4E-T (green).

(C) Western blots of E12.5 cortical lysates (input) immunoprecipitated (IP) with control IgG (IgG) or with anti-4E-T (4E-T), probed for eIF4E1 or 4E-T. Arrowheads denote the target proteins.

(D) High-magnification confocal images of cell bodies (left) and apical endfeet (right) of precursors in the E14.5 VZ, immunostained for eIF4E1 (green) and 4E-T (red). Arrows denote colocalized eIF4E1 and 4E-T, and white lines denote the boundary of the VZ and lateral ventricle (LV).

(E) Confocal images of precursors cultured two days and immunostained for 4E-T (green), eIF4E1 (red) and eIF4G (blue). The middle and bottom panels show progressively higher magnification images of the boxed areas. Arrows denote a granule positive for 4E-T and eIF4E1 and the arrowhead denotes a granule positive for eIF4E1 and eIF4G. A closed versus open arrow/arrowhead indicates that a granule is positive or negative for a marker.

(F) Quantification of images as in (E) for the percentage of 4E-T-positive foci colabeled for eIF4E1 or eIF4G. $^{**}p < 0.01$. $n \geq 15$ cells each.

(G) Western blots of HEK293 cells cotransfected with FLAG-tagged mouse 4E-T and control or 4E-T shRNAs (sh4E-T-1 or sh4E-T-2). The blot was probed for FLAG and reprobed for Erk1/2. Arrowheads denote target proteins.

(H) Cultured precursors were cotransfected with EGFP and control or 4E-T shRNA2 (sh4E-T) for 3 days and immunostained, and EGFP-positive cells expressing high 4E-T were quantified. $^{**}p < 0.01$; $n = 3$ experiments.

(I–M) E13/14 cortices were coelectroporated with EGFP and control shRNA or 4E-T shRNA2 (sh4E-T) and coronal cortical sections were immunostained 3 days later. (I) Sections immunostained for EGFP (green). (J–M) Quantification of EGFP-positive cells that expressed Pax6 (J); Ki67 (K); Satb2, Ctip2, or Tbr1 (L); or βIII-tubulin (M). $^{**}p < 0.01$; $n \geq 3$ embryos each.

(N) Western blots of HEK293 cells transfected with wild-type or Y30A FLAG-tagged mouse 4E-T, probed for FLAG, and reprobed for Erk1/2. Arrowheads denote target proteins.

(O–R) E13/14 cortices were coelectroporated with EGFP and control or 4E-T shRNA2 (sh4E-T) plus wild-type (WT) or Y30A 4E-T. Coronal cortical sections were immunostained 3 days later. (O) Sections immunostained for EGFP (green). (P–R) Quantification of EGFP-positive cells expressing Pax6 (P), Ki67 (Q), or Satb2 (R). $^{*}p < 0.05$, $^{**}p < 0.01$; $n \geq 4$ embryos each.

Sections in (B, D, I, and O) were counterstained with Hoechst (blue). Scale bars, 30 μm in (B), (I), and (O); 5 μm in (D); and 1 μm in (E). Error bars denote SEM. See also Figure S3.

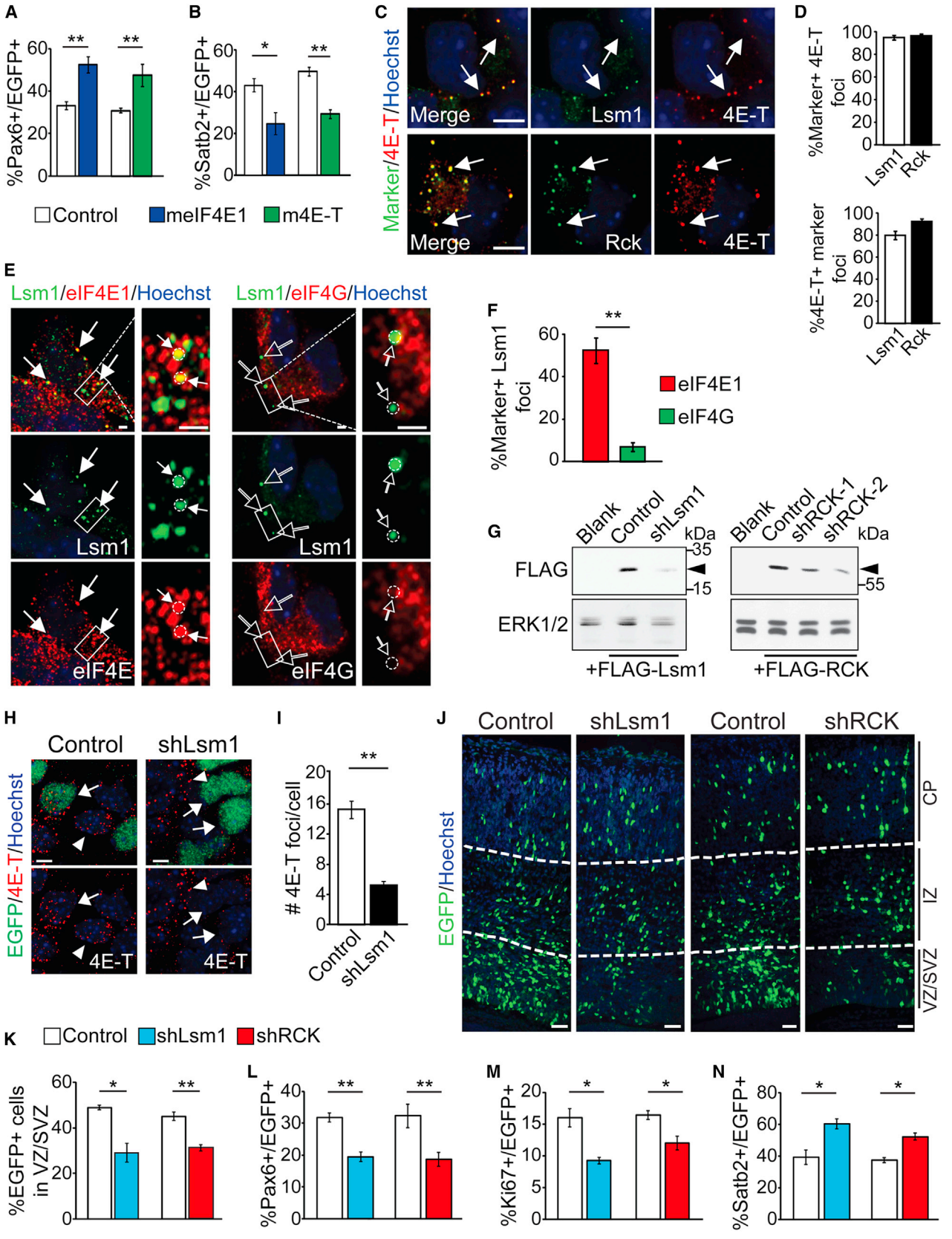

(legend on next page)

(FISH) for these mRNAs, coupled with immunocytochemistry for 4E-T on E15 cortical sections. *neurogenin1*, *neurogenin2*, and *neurod1* mRNAs were all enriched in cells of the VZ/SVZ, although the patterns of hybridization were distinct (Figure 7A), as shown previously (Visel et al., 2007). In contrast, *tle4* mRNA was appropriately enriched in cells of the CP (Figure 7A) (Yao et al., 1998). This hybridization was only seen with antisense, and not sense, probes (Figure S5A).

Combined FISH and 4E-T immunostaining showed that *neurogenin1*, *neurogenin2* and *neurod1* mRNAs all partially colocalized with 4E-T-positive foci (Figures 7B–7D). This localization was not exclusive; 4E-T was present in many granules that did not contain the mRNA of interest, and the converse was also true, with the mRNAs present in granules that did not contain 4E-T. We confirmed this colocalization with z stack analysis (Figures 7B–7D) and spectral scan analysis (Figure S5B).

We quantified the *neurogenin1* mRNA/4E-T colocalized foci in these sections (Figure 7E; Figure S5C); 30.5% ± 2.2% of *neurogenin1* mRNA foci colocalized with 4E-T. These were not, however, evenly distributed across the VZ/SVZ. The highest proportion of *neurogenin1*-mRNA-positive foci was found in the region at the interface of the VZ and SVZ (Figure 7E, bin 2; Figure 7F). In contrast, the highest proportion of *neurogenin1*-mRNA-positive, 4E-T-positive foci was in the apicalmost part of the VZ (Figure 7E, bin 1; Figure 7G). In this region, which is predominantly composed of radial precursors, almost 60% of *neurogenin1* mRNA foci were colocalized with 4E-T (Figure 7H).

As a control for this colocalization, we analyzed *glo1* mRNA, which was not enriched in the 4E-T immunoprecipitates and which encodes glyoxalase 1, a metabolic protein. FISH combined with 4E-T immunostaining showed that *glo1* mRNA was expressed throughout the E12 cortex and that only 11.6% ± 1.6% of total *glo1* mRNA foci colocalized with 4E-T (Figures S5D–S5F). This low proportion was constant over the entirety of the VZ/SVZ (Figure S5G), verifying the specificity of our analysis.

We next performed triple labeling for *neurogenin1* mRNA, 4E-T, and Neurogenin1 protein to ask whether precursors containing *neurogenin1* mRNA/4E-T complexes expressed Neurogenin1 protein (Figure 7I). This analysis showed that all Neurogenin1-protein-positive cells expressed *neurogenin1* mRNA. In addition, some cells were positive for the mRNA but not the protein, and this group contained *neurogenin1*-mRNA-positive, 4E-T-positive foci (Figure 7I). Quantification showed that these *neurogenin1* mRNA/4E-T foci were significantly enriched in the *neurogenin1*-mRNA-positive, protein-negative cells (Figure 7J), consistent with the idea that they were repressive in nature.

We performed a similar analysis for *neurogenin2* mRNA in the E12 cortex, a time point when it is predominantly found in cycling precursors (Shimojo et al., 2008). Quantification showed that 37.7% ± 1.6% of *neurogenin2* mRNA foci colocalized with 4E-T at this age (Figure 8A; Figure S6A). The highest proportion of *neurogenin2*-mRNA-positive foci was found at the interface of the VZ and SVZ (Figure 8A, bin 2; Figure 8B), but *neurogenin2*-mRNA-positive, 4E-T-positive foci were most enriched in the apicalmost region (Figure 8A, bin 1; Figure 8C) where there was almost 60% colocalization (Figure 8D). Triple labeling showed that all Neurogenin2-protein-positive cells also expressed *neurogenin2* mRNA but that some cells were only positive for the mRNA (Figure 8E). Quantification showed that almost 60% of the *neurogenin2* mRNA foci colocalized with 4E-T in cells that did not express Neurogenin2 protein, a proportion twice as high as in cells that expressed both mRNA and protein (Figure 8F).

Disruption of the 4E-T/eIF4E P-body-like Complexes Causes Aberrant Upregulation of Neurogenic bHLH Proteins

If the eIF4E1/4E-T/proneurogenic mRNA complexes defined here are repressive, then disruption of these complexes should cause aberrant translation of the neurogenic bHLH proteins. To test this prediction, we electroporated the E13/14 cortex with eIF4E1 or 4E-T shRNAs and immunostained electroporated cortices for Neurogenin1, Neurogenin2, or NeuroD1 proteins 2 days later (Figures 8G, 8I, and 8K; Figures S6B–S6D). About 15%–25% of electroporated cells expressed detectable

Figure 5. eIF4E and 4E-T Colocalize with the P-body Proteins Lsm1 and Rck, and Knockdown of Lsm1 or Rck Phenocopies the eIF4E and 4E-T Knockdowns

(A and B) E13/14 cortices were coelectroporated with EGFP and mouse eIF4E1 (meIF4E1) or 4E-T (m4E-T), and cortical sections were immunostained 3 days later. Sections were quantified for EGFP-positive cells that expressed Pax6 (A) or Satb2 (B). $^{*}p < 0.05$, $^{**}p < 0.01$; $n \geq 4$ embryos each.

(C and D) Cultured precursors were immunostained for 4E-T (red) and Lsm1 or Rck (both green, C), and analyzed for 4E-T-positive foci that colocalized with Lsm1 or Rck (D, top graph) or for Lsm1- or Rck-positive foci that colocalized with 4E-T (D, bottom graph). Arrows in (C) denote double-labeled granules. n = 20 cells each.

(E) Images of precursors cultured 2 days and immunostained for Lsm1 (green) and eIF4E1 (red, left panels) or eIF4G (red, right panels). Boxed areas are shown at higher magnification at the right. Closed arrows indicate foci positive for Lsm1 and eIF4E1, and open arrows indicate foci that are only positive for Lsm1.

(F) Quantification of images as in (E) for Lsm1-positive foci that colocalized with eIF4E1 or eIF4G. $^{**}p < 0.01$. n = 20 cells each.

(G) Western blots of HEK293 cells (Blank) cotransfected with FLAG-tagged mouse Lsm1 or Rck and control, Lsm1 or Rck shRNAs (shLsm1, shRck2). The blot was probed for FLAG and reprobed for Erk1/2. Arrowheads denote target proteins.

(H and I) Cultured precursors were cotransfected with EGFP and control or Lsm1 shRNA and immunostained 3 days later for EGFP (green) and 4E-T (red) (H), and the number of 4E-T-positive foci per transfected cell was counted (I). In (H), arrows and arrowheads denote transfected and nontransfected cells, respectively. $^{**}p < 0.01$. $n \geq 30$ cells each.

(J–N) E13/14 cortices were coelectroporated with EGFP and control, Lsm1, or Rck shRNAs (shLsm1, shRck), and cortical sections were immunostained 3 days later. (J and K) Sections were immunostained for EGFP (green, J), and EGFP-positive cells in the VZ/SVZ were counted (K). (L–N) Quantification of sections for EGFP-positive cells that expressed Pax6 (L), Ki67 (M), or Satb2 (N). $^{*}p < 0.05$; $^{**}p < 0.01$; $n \geq 3$ embryos each.

Sections or cells in (C), (E), (H), and (J) were counterstained with Hoechst (blue). Scale bars, 40 μm in (J); 5 μm in (C), (G), and (H); and 1 μm in (E). Error bars denote SEM.

See also Figure S4.

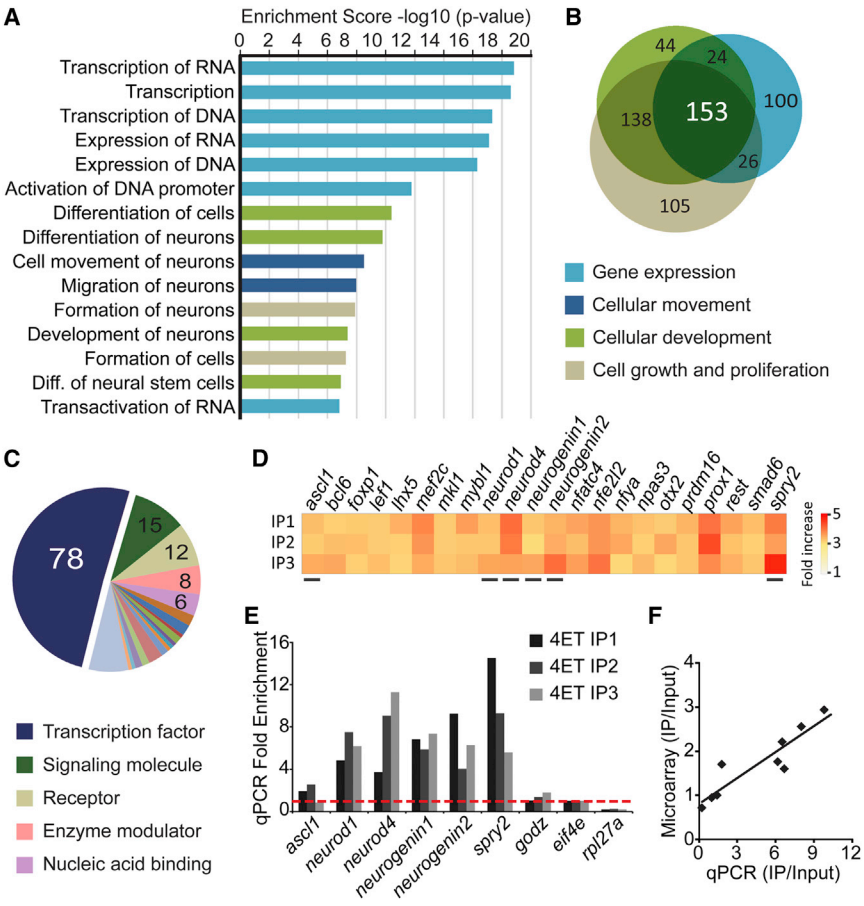

Figure 6. 4E-T Complexes in the Embryonic Cortex Are Enriched for mRNAs Encoding Transcription Factors that Regulate Neural Development

(A) Gene ontology and pathway analysis of mRNAs enriched in 4E-T immunoprecipitates from E12/13 cortex, as detected by microarray analysis. The top 15 ontology terms ranked by their enrichment p value (x axis) were color coded and classified into four major groups based on biological functions; gene expression, cellular movement, cellular development, and cell growth and proliferation. n = 3 independent control and 4E-T immunoprecipitate samples each (see Experimental Procedures).

(B) Venn diagram showing the number and overlap of genes that belonged to each of three top-ranked biological function groups, as seen in (A).

(C) A pie chart showing the 153 overlapping genes identified in (B) categorized based on their protein functions.

(D) A heat map of 22 of the transcription factors identified in (A–C) that have known functions in neurogenesis, showing their fold increase (immunoprecipitate/input) from three independent microarray experiments. Genes that were analyzed further are underlined. IP, immunoprecipitate.

(E) Validation of the selected target mRNAs highlighted in (D) by qPCR. Three independent 4E-T immunoprecipitates and their initial input samples were analyzed for *ascl1*, *neurod1*, *neurod4*, *neurogenin1*, *neurogenin2*, *sprouty2*, *godz*, *eif4e*, and *rpl27a* mRNAs. Relative fold enrichment of each of these mRNAs is shown and compared to the input (hatched red line). Enrichment of *godz* (1.0 ± 0.07 in microarray), *eIF4E* (0.94 ± 0.03 in microarray), and *rpl27a* (0.71 ± 0.03 in microarray) mRNAs served as controls.

(F) Correlation of enrichment values (immunoprecipitates/input) for the microarrays versus the qPCRs. Each point represents the average value from three 4E-T immunoprecipitates and their initial inputs for each of the mRNAs shown in (E). Pearson's correlation coefficient, p = 0.0006.

See also Table S1.

Neurogenin1, Neurogenin2, or NeuroD1 in control sections, but this increased to as much as 50% following eIF4E1 or 4E-T knockdown (Figures 8G–8L).

These data argue that 4E-T and eIF4E are necessary to repress translation of these neurogenic mRNAs. To ask if their localization to P-bodies was also important, we performed similar studies, knocking down Lsm1 or Rck. Analysis 2 days postelectroporation showed that Lsm1 or Rck knockdown almost doubled the proportion of EGFP-positive, Neurogenin1-positive, or Neurogenin2-positive cells (Figures 8M and 8N; Figures S6E and S6F). Together, these data support a model where radial precursors are transcriptionally primed to generate neurons but where a repressive eIF4E1/4E-T complex maintains them in an undifferentiated state by sequestering and inhibiting translation of proneurogenic mRNAs in association with P-body components (Figure 8O).

DISCUSSION

Data presented here indicate that translational regulation plays a key role during cortical neurogenesis. First, we define an eIF4E1/4E-T complex that represses neurogenesis and maintains the radial precursor state. Second, we show that this repressive complex is localized to P-body-like granules and that disruption of P-body proteins enhances neurogenesis and depletes precursors. Third, we show that the 4E-T complex binds mRNAs encoding regulators of transcription and cell differentiation, arguing that it represents a mechanism for globally repressing precursor differentiation. Finally, we show that the 4E-T-associated mRNAs include those encoding proneurogenic bHLHs such as the neurogenins. These 4E-T/*neurogenin* mRNA complexes are enriched in precursors that do not express Neurogenin proteins, and disruption of eIF4E, 4E-T, or P-body proteins causes aberrant derepression and translation of these bHLHs.

These findings support a model where neural precursors are transcriptionally primed to differentiate into neurons but where the relevant mRNAs are sequestered by a repressive eIF4E1/4E-T P-body complex, thereby inhibiting neurogenesis (Figure 8O). In this model, differentiation-promoting extrinsic cues would cause dissociation of this complex, leading to coordinated translation of not one but many proneurogenic proteins, thereby allowing rapid initiation of neurogenesis. Such a mechanism would also allow for phenotypic preprogramming since the repertoire of mRNAs bound to the eIF4E1/4E-T complex could

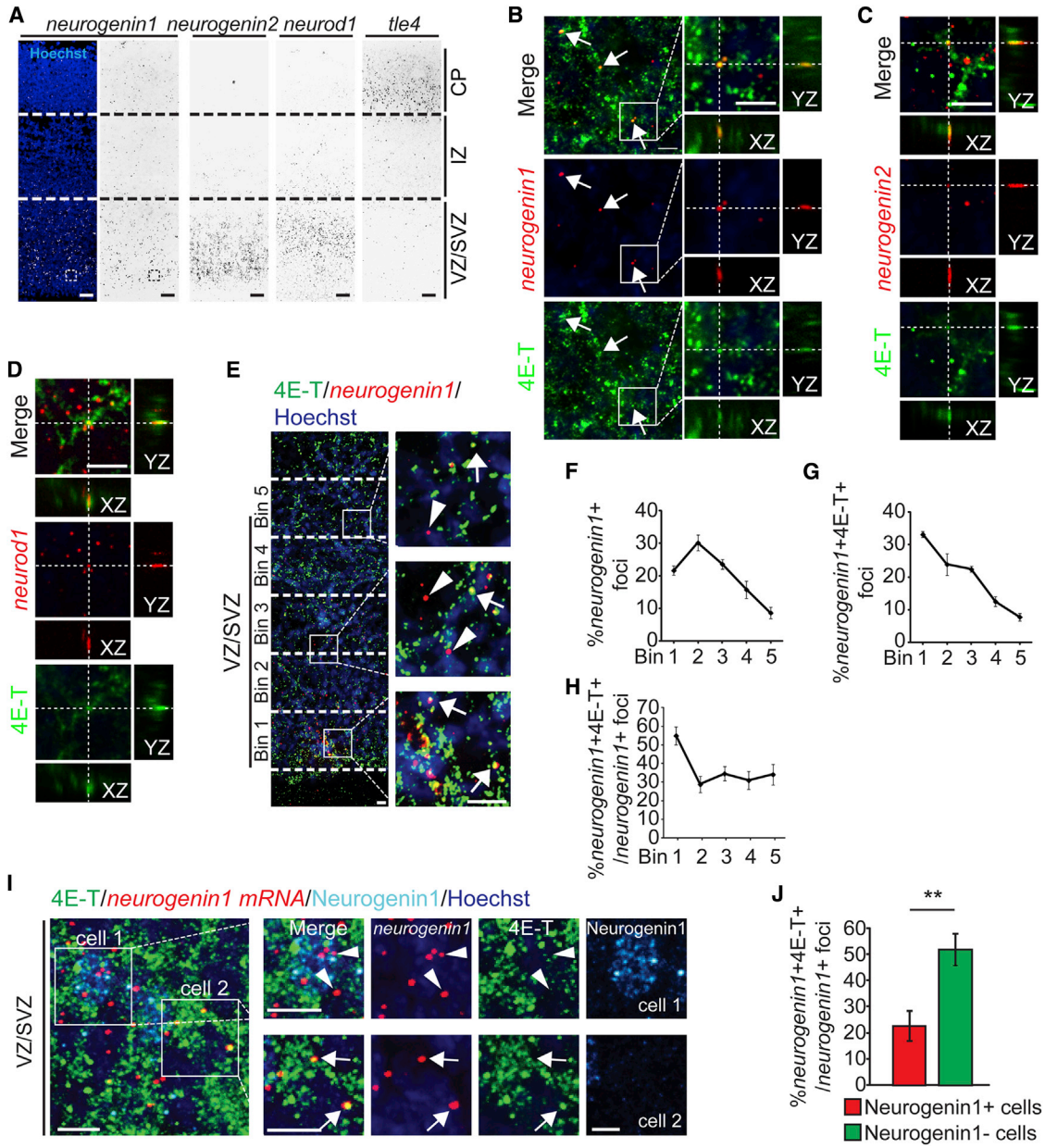

Figure 7. 4E-T Colocalizes with Neurogenic bHLHs in the Embryonic Cortex, and *neurogenin1* mRNA/4E-T Complexes Are Enriched in Neurogenin1-Protein-Negative Precursors

(A) FISH for *neurogenin1*, *neurogenin2*, *neurod1*, and *tle4* mRNAs in E15 coronal cortical sections.

(B) Higher magnification images of the boxed regions in the *neurogenin1* panels in (A), showing FISH for *neurogenin1* mRNA (red) and immunostaining for 4E-T (green). Arrows denote colocalized 4E-T and *neurogenin1* mRNA. Boxed regions are shown at higher magnification in the right panels, which also show colocalization of 4E-T and *neurogenin1* mRNA on the z axis (XZ and YZ), as indicated by hatched white lines.

(C and D) Higher magnification images of sections as in (A), with immunostaining for 4E-T (green) and FISH for *neurogenin2* mRNA (C) or *neurod1* mRNA (D). Hatched white lines show colocalization on the z axis (XZ and YZ).

(E) E15 cortical sections showing FISH for *neurogenin1* mRNA (red) and immunostaining for 4E-T (green). The VZ/SVZ is divided into five bins of identical width, and boxed regions are shown at higher magnification at the right. Arrows denote foci with colocalized *neurogenin1* mRNA and 4E-T, and arrowheads denote foci with only *neurogenin1* mRNA.

(F–H) Quantification of sections as in (E) for localization of *neurogenin1*-mRNA-positive foci (F) or foci colabeled for *neurogenin1* mRNA and 4E-T (G), or for the proportion of *neurogenin1*-mRNA-positive foci colocalized with 4E-T in each bin (H).

(I) E15 cortical section immunostained for 4E-T (green) and Neurogenin1 (bluish white) and hybridized for *neurogenin1* mRNA (red). Boxed cells are shown at higher magnification at the right. Arrowheads denote *neurogenin1* mRNA foci that are negative for 4E-T in a Neurogenin1-positive cell, and arrows denote double-positive foci in a Neurogenin1-negative cell.

(legend continued on next page)

be transcriptionally "personalized" either in precursors with different fate biases or in the same precursors producing different neural cell types at different developmental time points. Moreover, this model would allow for asymmetric neurogenic divisions; both daughter cells might receive the same repressive parental mRNP complexes, but only one daughter would be exposed to prodifferentiative environmental signals that would promote complex dissociation and translational derepression of neurogenic mRNAs.

One surprising finding is that the eIF4E1/4E-T targets include proneurogenic bHLH mRNAs. The Neurogenins and NeuroDs promote neurogenesis and neuronal differentiation by inducing a broad cluster of neurogenesis-related genes (Imayoshi and Kageyama, 2014; Seo et al., 2007). These potent bHLH proteins are short lived, and their levels and activity are modulated at multiple levels, ranging from transcription to phosphorylation. One particularly intriguing regulatory mechanism involves protein oscillations that are thought to control precursor proliferation versus differentiation. These oscillations, which are trancriptionally defined, are best characterized for Hes1, Ascl1, and Olig2 (Imayoshi et al., 2013; Imayoshi and Kageyama, 2014) but also occur for Neurogenin2 (Shimojo et al., 2008). We suggest that the neurogenic bHLHs are coregulated by the translational control mechanisms we report here and that different precursor populations may use either or both mechanisms to temporally and spatially regulate neurogenesis.

Our data indicate that the proneural bHLHs are not the only relevant proteins translationally regulated by the eIF4E1/4E-T complex. Remarkably, 17.6% of the 4E-T-associated mRNAs encode transcription factors, and many of these regulate neuronal differentiation, including Mef2C, Prox1, Lef1, and Npas3. The 4E-T-enriched population also included many mRNAs for proteins other than transcription factors that regulate neurogenesis and neuronal differentiation or migration such as Slit2, ASPM, and Sema3A. These findings suggest that the eIF4E1/4E-T repressive complexes act to orchestrate neuronal development by the timely and stepwise release and derepression of different groups of mRNAs.

One surprising finding reported here is that eIF4E1 knockdown disrupts the eIF4E1/4E-T/*neurogenin* mRNA complex, but *neurogenin* mRNA translation still occurs. This result suggests that a higher level of eIF4E1 is required to maintain the repressive complex than to initiate translation. Alternatively, radial precursors also express eIF4E2 and eIF4E3 mRNAs (G.Y., D.R.K., and F.D.M., unpublished data), and another eIF4E family member may mediate translational initiation following eIF4E1 knockdown.

If 4E-T is repressive, and eIF4E1 has both positive and negative roles, then this would explain differences in their knockdown phenotypes. In particular, only eIF4E1 knockdown alters neuronal positioning, presumably because of the lack of translation of proteins important for migration. How then does 4E-T repress translation? 4E-T does not apparently bind mRNAs directly, but it represses translation when artificially tethered to mRNA (Kamenska et al., 2014), suggesting that it needs an intermediary protein to bring it to its target mRNAs. The identity of the relevant mammalian 4E-T binding protein(s) is still unknown, but in *Xenopus*, 4E-T binds to the 3′ UTR binding protein CPEB as part of a translational repressor complex (Minshall et al., 2007). Intriguingly, CPEB family members repress translation in mammalian neurons, and mice lacking CPEB1 show deficits in neural circuit formation (Darnell and Richter, 2012).

Our data indicate that the 4E-T repressive complexes are localized to P-bodies and that this localization is important for repressing neurogenesis. P-bodies contain mRNAs, microRNAs, translational repression complexes, and mRNA decay enzymes, and they regulate the decay and reversible translational repression of subsets of mRNAs (Eulalio et al., 2007). Two important proteins for P-bodies are Lsm1 and Rck/p54 (Kulkarni et al., 2010). We show here that these proteins localize with 4E-T, and our knockdown studies indicate that they are important for repressing neurogenesis. While disruption of P-body proteins likely has effects that are broader than disruption of 4E-T alone, our data are consistent with the conclusion that the P-body localization is important for the eIF4E1/4E-T repressive complex.

One final question is whether perturbation of eIF4E/4E-T repressive complexes plays any role in humans with ASD, where eIF4E expression is increased due to mutation of its promoter (Neves-Pereira et al., 2009). In mouse models, increased eIF4E activity caused aberrant ASD-like behaviors and perturbed circuitry (Santini et al., 2013; Gkogkas et al., 2013). Since we show here that ectopic expression of eIF4E1 in cortical precursors perturbed neurogenesis, then it is feasible that similar perturbations in humans could contribute to neuroanatomical and behavioral changes. Moreover, since we show that 4E-T is expressed in developing neurons, then it is possible, and perhaps even likely, that the eIF4E/4E-T repressive complexes we have defined here might be equally important in directly shaping synaptic connectivity.

EXPERIMENTAL PROCEDURES

Animals

Animal use was approved by the Animal Care Committee of the Hospital for Sick Children in accordance with CCAC policies. CD1 mice (Charles River Laboratories) were used for all experiments.

Cell Culture and Transfections

E12/13 murine cortical precursors and HEK293 cells were cultured and transfected essentially as described elsewhere (Gauthier et al., 2007). For co-transfections, a 1:3 ratio of nuclear EGFP plasmid to shRNA or overexpression plasmids was used. Further details and plasmids are in the Supplemental Information.

Protein Immunoprecipitation and Immunoblotting

Freshly dissected E12/13 murine cerebral cortices were used for immunoprecipitations. Western blots were performed as previously described (Yang et al., 2013). Further details are in the Supplemental Information.

(J) Quantification of images as in (I) for the proportion of *neurogenin1*-mRNA-positive foci that colabel for 4E-T in cells that are Neurogenin1 protein positive and negative. $^{**}p < 0.01$. n = 25 cells each.

Sections in (A), (E), and (I) were counterstained with Hoechst (blue). Scale bars, 50 μm in (A) and 10 μm in (B), (C), (D), (E), and (I). Error bars denote SEM. See also Figure S5.

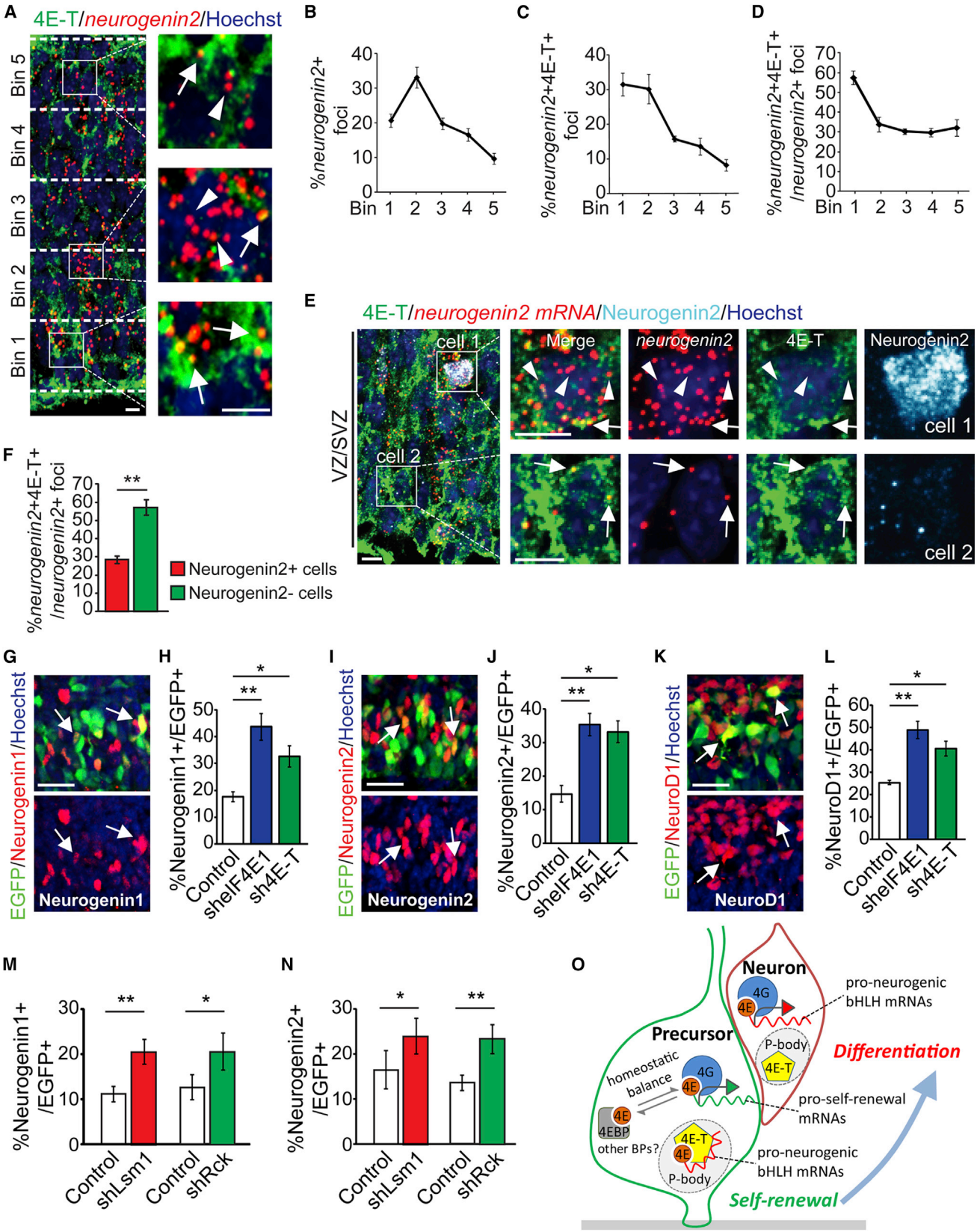

(legend on next page)

PCR

Total mRNA was isolated with the Magnetic mRNA Isolation Kit (New England Biolabs), following manufacturer's instructions. cDNA was synthesized from total mRNA with the First Strand cDNA Synthesis Kit (Thermo Scientific). Details of amplification and primers are in the Supplemental Information.

In Utero Electroporation

In utero electroporation was performed as described elsewhere (Gauthier et al., 2007; Zander et al., 2014). The nuclear EGFP expression construct was coelectroporated with shRNAs or overexpression constructs at a 1:3 ratio (or, when two additional plasmids were coelectroporated, at a 1:2:2 ratio) for a total of 4 μg DNA. Plasmids are described in the Supplemental Information.

Immunostaining and Analysis

Immunocytochemistry and analysis of cell culture and brain sections were performed as previously described (Vessey et al., 2012; Zander et al., 2014). Antibodies and further details of immunostaining are given in the Supplemental Information. Cells grown on glass coverslips were analyzed with a Zeiss Axioplan2 microscope; at least 300 cells from different fields were counted per condition, and at least three independent experiments were analyzed. For clonal experiments, 200–450 clones were analyzed per condition per experiment. For quantification of eIF4E1 or 4E-T levels in cortical precursor cultures, cells with detectable/strong intensity of eIF4E1 staining or with obvious 4E-T granules were considered to be positive. For analysis of 4E-T granules in Lsm1 knockdown cells, strongly immunopositive 4E-T foci were quantified. To analyze protein colocalization in cultured cells, cultures were imaged with a 100× objective on an Olympus IX81 fluorescence microscope equipped with a Hamamatsu C9100-13 back-thinned EM-CCD camera and Okogawa CSU X1 spinning disk confocal scan head. Brightly positive 4E-T, Lsm1-positive, and Rck-positive granules from z-stacked images were selected, and only those colocalized foci that were verified in each section of the stack were counted. For analysis of in utero electroporations, three to four anatomically matched sections per brain from at least three embryos were imaged with a 20× objective on the spinning disk confocal microscope. Images were processed with Volocity software (PerkinElmer), ImageJ (NIH), and Adobe Photoshop. Pax6, Tbr2, and Hoechst staining were used to define the VZ, SVZ, and CP, respectively.

RNA Immunoprecipitation and Microarray Analysis

E12/13 cortices were analyzed with the Magna RIP RNA-Binding Protein Immunoprecipitation Kit as per the manufacturer's instructions (Millipore). Input lysates were precleared with protein A/G beads and incubated with 5 μg mouse anti-4E-T (Abnova) or normal mouse IgG (Millipore) for 3 hr at 4°C. Total RNA was isolated, extracted with phenol/chloroform, and quality checked on a BioAnalyzer (Agilent). RNA samples from three biological replicates each of input and IgG control and 4E-T immunoprecipitates were amplified using the NuGEN Pico protocol (NuGEN) and analyzed on Mouse Gene 2.0 ST Arrays (Affymetrix) (GEO accession number GSE61729). The raw microarray data were normalized using robust multiarray analysis in the Expression Console (Affymetrix) program. Probe sets of annotated transcripts with expression levels in the top 80% of total RNA input samples (n = 21,630 probe sets) were compared with immunoprecipitate samples. Transcripts showing at least a 1.5-fold change in 4E-T immunoprecipitates versus total input RNA were analyzed further. Nonspecific RNA candidates from IgG immunoprecipitates were subtracted from the 4E-T immunoprecipitates to minimize off-target binding (Kusek et al., 2012). 4E-T-enriched candidates were statistically compared to input, and p values were adjusted using the Benjamini-Hochberg method. The enriched probe sets were analyzed using Ingenuity Pathway Analysis (QIAGEN) and the PANTHER Classification System.

FISH

FISH was performed with probes targeting *neurogenin1* (National Center for Biotechnology Information [NCBI] Nucleotide Reference Sequence [RefSeq] database accession number NM_010896.2), *neurogenin2* (NCBI Nucleotide RefSeq accession number NM_009718.2), *neurod1* (NCBI Nucleotide RefSeq accession number NM_010894.2), *tle4* (NCBI Nucleotide RefSeq accession number NM_011600.2), and *glo1* (NCBI Nucleotide RefSeq accession number NM_025374.3) using the RNAscope kit (Advanced Cell Diagnostics), according to the manufacturer's instructions (described in the Supplemental Information). After FISH, immunostaining was performed for 4E-T. The z stacks of confocal images were taken with an optical slice thickness of 0.1 μm, with a 60× objective on the spinning disk confocal microscope. We quantified 200–800 mRNA granules in 80–300 z-stacked images from random regions of the VZ/SVZ. For coimmunodetection of Neurogenin1 or Neurogenin2, brains were fixed in 4% paraformaldehyde overnight and snap frozen. Twenty-five cells in each category were randomly chosen for *neurogenin* mRNA/4E-T colocalization quantification, and all foci in those cells were counted.

Statistics

All data were expressed as the mean ± SEM. Statistical analysis was performed using a two-tailed Student's t test or, where relevant, ANOVA with Tukey or Dunnett post hoc tests, unless otherwise indicated.

ACCESSION NUMBERS

The GEO accession number for the microarray data reported in this paper is GSE61729.

Figure 8. *neurogenin2* mRNA/4E-T Complexes Are Enriched in Neurogenin2-Protein-Negative Precursors, and Knockdown of eIF4E, 4E-T, or P-body Proteins Derepresses Neurogenic bHLH Translation

(A) E12 cortical section showing FISH for neurogenin2 mRNA (red) and immunostaining for 4E-T (green). The VZ/SVZ is divided into five bins of identical width, and boxed regions are shown at higher magnification to the right. Arrows denote foci positive for both *neurogenin2* mRNA and 4E-T, and arrowheads denote foci with only *neurogenin2* mRNA.

(B–D) Quantification of sections as in (A) for distribution of *neurogenin2*-mRNA-positive foci (B) or for foci colabeled for *neurogenin2* mRNA and 4E-T (C), or for the relative proportion of *neurogenin2*-mRNA-positive foci that colocalize with 4E-T in each bin (D).

(E) E12 cortical section immunostained for 4E-T (green) and Neurogenin2 (bluish white) and hybridized for *neurogenin2* mRNA (red). Boxed cells are shown at higher magnification at the right. Arrowheads denote *neurogenin2*-mRNA-only foci, and arrows denote double-positive foci.

(F) Quantification of images as in (E) for the proportion of *neurogenin2*-mRNA-positive foci that are colocalized with 4E-T in cells that are Neurogenin2 protein positive and negative. $^{**}p < 0.01$. n = 25 cells each.

(G–L) E13/14 cortices were coelectroporated with EGFP and control, eIF4E1, or 4E-T shRNAs (sheIF4E1 and sh4E-T). Two days later, coronal cortical sections were immunostained for EGFP (green) and for Neurogenin1 (red, G), Neurogenin2 (red, I), or NeuroD (red, K). Sections were analyzed for the proportion of EGFP-positive cells that expressed Neurogenin1 (H), Neurogenin2 (J), or NeuroD (L). Arrows in (G), (I), and (K) denote double-labeled cells. $^{*}p < 0.05$; $^{**}p < 0.01$; $n \geq 3$ embryos each.

(M and N) E13/14 cortices were coelectroporated with EGFP and control, Lsm1, or Rck shRNAs (shLsm1 and shRck). Two days later, immunostained cortical sections were analyzed for the proportion of EGFP-positive cells that expressed Neurogenin1 (M) or Neurogenin2 (N). $^{*}p < 0.05$; $^{**}p < 0.01$; n = 3 embryos each.

(O) Schematic of the proposed model. Sections in (A),(E), (G), (I), and (K) were counterstained with Hoechst (blue). Scale bars, 5 μm in (A) and (E) and 30 μm in (E), (G), and (I). Error bars denote SEM.

See also Figure S6.

SUPPLEMENTAL INFORMATION

Supplemental Information includes Supplemental Experimental Procedures, six figures, and one table and can be found with this article online at http://dx.doi.org/10.1016/j.neuron.2014.10.022.

AUTHOR CONTRIBUTIONS

G.Y. conceptualized, designed, and analyzed the experiments and cowrote the paper. C.A.S. supervised analysis of the RNA immunoprecipitation-microarray (chip) data. D.R.K. and F.D.M. conceptualized and designed experiments, analyzed data, and cowrote the paper.

ACKNOWLEDGMENTS

This work was funded by Canadian Institutes of Health Research grant MOP-125945 to D.R.K. and F.D.M.; a Multi-Investigator Research Initiative grant from Brain Canada to F.D.M; and a Natural Sciences and Engineering Research Council Discovery Grant to C.A.S. F.D.M. is a Howard Hughes Medical Institute Senior International Research Scholar, and F.D.M. and D.R.K. hold Canada Research Chairs. G.Y. is funded by a Brain Canada Mental Health Fellowship. We thank Sarah Burns and Anastassia Voronova for their help and Dr. Howard Lipshitz for advice and input.

Accepted: September 29, 2014
Published: November 6, 2014

REFERENCES

Andrei, M.A., Ingelfinger, D., Heintzmann, R., Achsel, T., Rivera-Pomar, R., and Lührmann, R. (2005). A role for eIF4E and eIF4E-transporter in targeting mRNPs to mammalian processing bodies. RNA *11*, 717–727.

Bertrand, N., Castro, D.S., and Guillemot, F. (2002). Proneural genes and the specification of neural cell types. Nat. Rev. Neurosci. *3*, 517–530.

Darnell, J.C., and Richter, J.D. (2012). Cytoplasmic RNA-binding proteins and the control of complex brain function. Cold Spring Harb. Perspect. Biol. *4*, a012344.

Eulalio, A., Behm-Ansmant, I., and Izaurralde, E. (2007). P bodies: at the crossroads of post-transcriptional pathways. Nat. Rev. Mol. Cell Biol. *8*, 9–22.

Ferraiuolo, M.A., Basak, S., Dostie, J., Murray, E.L., Schoenberg, D.R., and Sonenberg, N. (2005). A role for the eIF4E-binding protein 4E-T in P-body formation and mRNA decay. J. Cell Biol. *170*, 913–924.

Gauthier, A.S., Furstoss, O., Araki, T., Chan, R., Neel, B.G., Kaplan, D.R., and Miller, F.D. (2007). Control of CNS cell-fate decisions by SHP-2 and its dysregulation in Noonan syndrome. Neuron *54*, 245–262.

Gkogkas, C.G., Khoutorsky, A., Ran, I., Rampakakis, E., Nevarko, T., Weatherill, D.B., Vasuta, C., Yee, S., Truitt, M., Dallaire, P., et al. (2013). Autism-related deficits via dysregulated eIF4E-dependent translational control. Nature *493*, 371–377.

Imayoshi, I., and Kageyama, R. (2014). bHLH factors in self-renewal, multipotency, and fate choice of neural progenitor cells. Neuron *82*, 9–23.

Imayoshi, I., Isomura, A., Harima, Y., Kawaguchi, K., Kori, H., Miyachi, H., Fujiwara, T., Ishidate, F., and Kageyama, R. (2013). Oscillatory control of factors determining multipotency and fate in mouse neural progenitors. Science *342*, 1203–1208.

Jackson, R.J., Hellen, C.U., and Pestova, T.V. (2010). The mechanism of eukaryotic translation initiation and principles of its regulation. Nat. Rev. Mol. Cell Biol. *11*, 113–127.

Kamenska, A., Lu, W.T., Kubacka, D., Broomhead, H., Minshall, N., Bushell, M., and Standart, N. (2014). Human 4E-T represses translation of bound mRNAs and enhances microRNA-mediated silencing. Nucleic Acids Res. *42*, 3298–3313.

Kulkarni, M., Ozgur, S., and Stoecklin, G. (2010). On track with P-bodies. Biochem. Soc. Trans. *38*, 242–251.

Kusek, G., Campbell, M., Doyle, F., Tenenbaum, S.A., Kiebler, M., and Temple, S. (2012). Asymmetric segregation of the double-stranded RNA binding protein Staufen2 during mammalian neural stem cell divisions promotes lineage progression. Cell Stem Cell *11*, 505–516.

Minshall, N., Reiter, M.H., Weil, D., and Standart, N. (2007). CPEB interacts with an ovary-specific eIF4E and 4E-T in early Xenopus oocytes. J. Biol. Chem. *282*, 37389–37401.

Napoli, I., Mercaldo, V., Boyl, P.P., Eleuteri, B., Zalfa, F., De Rubeis, S., Di Marino, D., Mohr, E., Massimi, M., Falconi, M., et al. (2008). The fragile X syndrome protein represses activity-dependent translation through CYFIP1, a new 4E-BP. Cell *134*, 1042–1054.

Neves-Pereira, M., Müller, B., Massie, D., Williams, J.H., O'Brien, P.C., Hughes, A., Shen, S.B., Clair, D.S., and Miedzybrodzka, Z. (2009). Deregulation of EIF4E: a novel mechanism for autism. J. Med. Genet. *46*, 759–765.

Novotny, I., Podolská, K., Blazíková, M., Valásek, L.S., Svoboda, P., and Stanek, D. (2012). Nuclear LSm8 affects number of cytoplasmic processing bodies via controlling cellular distribution of Like-Sm proteins. Mol. Biol. Cell *23*, 3776–3785.

Rau, M., Ohlmann, T., Morley, S.J., and Pain, V.M.J. (1996). A reevaluation of the cap-binding protein, eIF4E, as a rate-limiting factor for initiation of translation in reticulocyte lysate. J. Biol. Chem. *271*, 8983–8990.

Rhoads, R.E. (2009). eIF4E: new family members, new binding partners, new roles. J. Biol. Chem. *284*, 16711–16715.

Santini, E., Huynh, T.N., MacAskill, A.F., Carter, A.G., Pierre, P., Ruggero, D., Kaphzan, H., and Klann, E. (2013). Exaggerated translation causes synaptic and behavioural aberrations associated with autism. Nature *493*, 411–415.

Seo, S., Lim, J.W., Yellajoshyula, D., Chang, L.W., and Kroll, K.L. (2007). Neurogenin and NeuroD direct transcriptional targets and their regulatory enhancers. EMBO J. *26*, 5093–5108.

Shimojo, H., Ohtsuka, T., and Kageyama, R. (2008). Oscillations in notch signaling regulate maintenance of neural progenitors. Neuron *58*, 52–64.

Sonenberg, N., and Hinnebusch, A.G. (2009). Regulation of translation initiation in eukaryotes: mechanisms and biological targets. Cell *136*, 731–745.

Tsui, D., Vessey, J.P., Tomita, H., Kaplan, D.R., and Miller, F.D. (2013). FoxP2 regulates neurogenesis during embryonic cortical development. J. Neurosci. *33*, 244–258.

Vessey, J.P., Amadei, G., Burns, S.E., Kiebler, M.A., Kaplan, D.R., and Miller, F.D. (2012). An asymmetrically localized Staufen2-dependent RNA complex regulates maintenance of mammalian neural stem cells. Cell Stem Cell *11*, 517–528.

Visel, A., Carson, J., Oldekamp, J., Warnecke, M., Jakubcakova, V., Zhou, X., Shaw, C.A., Alvarez-Bolado, G., and Eichele, G. (2007). Regulatory pathway analysis by high-throughput in situ hybridization. PLoS Genet. *3*, 1867–1883.

Wang, J., Weaver, I.C., Gauthier-Fisher, A., Wang, H., He, L., Yeomans, J., Wondisford, F., Kaplan, D.R., and Miller, F.D. (2010). CBP histone acetyltransferase activity regulates embryonic neural differentiation in the normal and Rubinstein-Taybi syndrome brain. Dev. Cell *18*, 114–125.

Yang, G., Zhou, X., Zhu, J., Liu, R., Zhang, S., Coquinco, A., Chen, Y., Wen, Y., Kojic, L., Jia, W., and Cynader, M.S. (2013). JNK3 couples the neuronal stress response to inhibition of secretory trafficking. Sci. Signal. *6*, ra57.

Yao, J., Liu, Y., Husain, J., Lo, R., Palaparti, A., Henderson, J., and Stifani, S. (1998). Combinatorial expression patterns of individual TLE proteins during cell determination and differentiation suggest non-redundant functions for mammalian homologs of Drosophila Groucho. Dev. Growth Differ. *40*, 133–146.

Zander, M.A., Burns, S.E., Yang, G., Kaplan, D.R., and Miller, F.D. (2014). Snail coordinately regulates downstream pathways to control multiple aspects of mammalian neural precursor development. J. Neurosci. *34*, 5164–5175.